JOURNAL OF THEORETICAL AND APPLIED MECHANICS
60, 4, pp. 659-671, Warsaw 2022
https://doi.org/10.15632/jtam-pl/155045

FORCE MECHANISM AND CONCEPTUAL DESIGN OF REINFORCED CONCRETE SHORT BEAM WITHOUT WEB REINFORCEMENT

Yi-Jun Chen, Hu-Zhi Zhang, Bei-Rong Lu, Yao-Sen Huang
School of Civil Engineering, Hunan University of Science and Technology, Xiangtan, China
Corresponding author Hu-Zhi Zhang, e-mail: zhanghz_hnu@163.com

Topology Optimization and Finite Element Analysis were carried out for reinforced concrete short beams to reveal the force mechanism. The results show that load-transfer paths for the beams can evolve from Bi-directional Evolutionary Structural Optimization and be mechanically supported by the Michell criterion. In the beams, the distribution of a high--stress compression area appears as a truss under a concentrated load and a tie-arch under a uniform load. The beams do not have much higher bearing capacity but can consume many more materials. Consequently, new design ideas were recommended based on the load transfer paths obtained by Topology Optimization.

Keywords: reinforced concrete short beam, topology optimization, conceptual design, load--transfer path, Michell criterion

1. Introduction

The current American Code (ACI Committee 318, 2019) generally defines Reinforced Concrete (RC) deep beams as their span-depth ratios are less than 4, while the current Chinese Code GB 50010-2010 (2016) defines those less than 5 as RC deep flexural members. In fact, they both can classify the beam members which do not conform to the plane section assumption. In that case, their normal stress is nonlinear and the shear stress might be a controlling factor for failure. Chinese Code GB 50010-2010 (2016) even further defines RC short beams as simply--supported beams with a span-depth ratio between 2 and 5, as well as continuous ones between 2.5 and 5. They are mostly used as structural components that provide high bearing capacity in engineering.

Empirical and semi-empirical design methods have been widely used in the reinforcement layout design of RC short beams in recent years, and even recommended by some national or regional codes, such as Appendix G of Chinese Code GB 50010-2010 (2016). In terms of reliability, many scholars have accomplished a large number of experiments and simulation studies. For instance, Uenaka and Tsunokake (2017) investigated bending shear characteristics of RC beams through an asymmetric four-point loading test and presented a method of prediction of simple shear capacity of the beam. Rombach (2011) discussed discrepancies between the experiment and simulation of RC deep flexural members, and obtained several suggestions on model building. Magnucki *et al.* (2017) found that there were few differences in the results of shear stress and deformation of RC short beams, using either Finite Element Analysis (FEA) or trigonometric series method. Díaz *et al.* (2020) recommended an advanced safety assessment method of combining nonlinear FEA with the reliability theory for the RC short beam design. All these researches have provided a lot of experience for the design of RC short beams, and also improved the accuracy of empirical and semi-empirical design methods. Nevertheless, for these methods, the fundamental problem of lack of a mechanical support has still not been solved.

As a result, numerous design methods based on stress distribution have become popularized, and the Strut-and-Tie Model (STM) method is most explored based on the plastic lower bound solution. Many scholars confirmed that it is feasible to guide the reinforcement layout design of RC short beams and other deep flexural members. Chen *et al.* (2018) developed a novel cracking STM to predict the shear strength of a RC short beam. Ismail *et al.* (2018) summarized the application of STMs for the design of RC beams and evaluated current formulations of effective factors. The STM method has a sound basis in mechanics since STMs can indicate load-transfer paths within members. However, there are still difficulties with the establishment of STMs.

Topology Optimization (TO), as a method to obtain the optimal distribution of materials (Bendsøe amd Sigmund, 2003), provides a new idea to solve this problem. The heuristic TO (Dorn *et al.*, 1964; Bendsøe and Kikuchi, 1988; Bendsøe, 1989) is one of the most concise and practical algorithms, such as Evolutionary Structural Optimization (ESO-type) algorithm (Xie and Steven, 1993) which has been applied in many engineering fields. Bi-directional Evolutionary Structural Optimization (BESO) (Querin *et al.*, 1998) can be used to evolve into an optimal structure by removing inefficient materials and adding efficient materials simultaneously and iteratively from the initial design domain, based on FEA. Huang and Xie (2007) introduced a sensitivity filter into BESO so that the design solutions became mesh-independent. The latest version of the BESO (Xia *et al.*, 2018) method has shown promising performance when applying for a wide range of structural design problems including stiffness and frequency optimization, nonlinear material and large deformation, energy absorption, multiple materials, multiple constraints, periodic structures, and so on. Jewett and Carstensen (2019) tested three RC short beams, and stated that the ones which were automatically generated with reinforcement layouts had an increased stiffness and strength by using a TO framework, compared with that designed with a conventional STM. The efficient element retained in the process of TO can essentially reflect the load-transfer paths of members (Kotsovos, 1988), which provides a new idea for the stress design method of deep flexural members such as short beams.

Therefore, the paper starts with TO to seek the theoretical support for the topologies of RC short beams. The load-transfer paths of the short beams are ascertained through FEA and then their force mechanisms are revealed as well. Some new ideas of conceptual design are also proposed for short beams.

2. TO for a short beam

2.1. The basic idea and implementation of TO

The static behavior of a finite element model structure based on the BESO method is given as

$$\mathbf{Ku} = \mathbf{P} \tag{2.1}$$

where $\mathbf{K}$ is the global stiffness matrix, $\mathbf{u}$ is the displacement vector and $\mathbf{P}$ is the load vector.

The stiffness optimization problem (Yang *et al.*, 2002) can be written as

$$\text{minimize:} \qquad f = C(x) = \mathbf{P}^{\mathrm{T}}\mathbf{u} \tag{2.2}$$

$$\text{subject to;} \qquad g = \sum_{i=1}^{n} W_i x_i \leqslant W^* \qquad x_i \in \{0,1\} \tag{2.3}$$

where $C(x)$ is the mean compliance, W_i is mass the of element i, W^* is the prescribed total mass, x_i is the binary design variable indicating element presence (1) or absence (0), and n is the total number of structural elements.

The sensitivity analysis is to evaluate the change in the mean compliance ΔC by removing or adding an element. The gradient of the objective function with respect to individual element density can be easily derived by the adjoint method (Bendsøe and Sigmund, 2003). An element sensitivity number is calculated by

$$\alpha_i = \Delta C = \mathbf{u}_i^{\mathrm{T}} \mathbf{K}_i \mathbf{u}_i \tag{2.4}$$

where symbols with the subscript i are element entities, α_i is called the sensitivity number and $\alpha_i/2$ represents the element strain energy. In the case of displacement constraints, $\mathbf{u}_i$ is the element displacement vector of the real load; $\mathbf{K}_i$ is the element stiffness matrix.

The rejection ratio (RR) and inclusion ratio (IR) are used as a part of the algorithm which decides whether the material will be either removed or added (Querin *et al.*, 2000). Elements can be removed from the under-stressed regions if they satisfy

$$\sigma_e \leqslant RR\sigma_{max} \tag{2.5}$$

and added to the structure if they satisfy

$$\sigma_e \geqslant IR\sigma_{max} \tag{2.6}$$

where σ_e is the element von Mises stress or other selected criterion, σ_{max} is the maximum von Mises stress, RR and IR can be calculated by

$$\begin{aligned} RR &= r_0 + r_1 SS + a_{RR} ON \qquad 0 \leqslant RR \leqslant 1 \\ IR &= i_0 + i_1 SS + a_{IR} ON \qquad 0 \leqslant IR \leqslant 1 \end{aligned} \tag{2.7}$$

where $r_0 = 0$ and $i_0 = 1$; r_1 and i_1 are constants determined from numerical experience, normally $r_1 = 0.001$ and $i_1 = 0.01$; a_{RR} and a_{IR} are oscillatory number constants determined from numerical experience, normally $a_{RR} = 0.01$ and $a_{IR} = 0.1$. Further, SS is the steady state number and ON is the oscillation number.

If a state is reached where no element in the design domain can satisfy either Eq. (2.5) or (2.6), a steady state has been reached. For the optimization process to continue, the SS is incremented by 1 and the equations are repeated. When a group of elements are removed and added back to the structure iteration after iteration, an oscillatory state has been reached. The ON is then incremented by 1 and the equations are repeated. The details of the BESO with stiffness and displacement constraints are consistent with the way in the references (Yang *et al.*, 2002).

2.2. Topologies

For two identical RC short beams, each of them has a length of 3000 mm, a height of 1000 mm and a thickness of 200 mm. The strength grade of their concrete was designed with Chinese C30: the characteristic cube compressive strength reached 30 MPa with an accumulated frequency of 95% in the tests. Meanwhile, both Young's elastic modulus and Poisson's ratio are specified as 30 GPa and 0.2 respectively in Chinese C30. To the first beam, a concentrated load of 340 kN on the top of the mid-span was applied, and a uniform load of 1500 kN/m^2 on the whole top to the other one.

BESO was carried out to obtain topologies by using MATLAB programming with a plane--stressed rectangular element of 4-nodes, composite material of RC and sensitivity of element strain energy. The initial topologies of the two beams are shown in Fig. 1a. They are discretized into 25 mm×25 mm quadrangle elements. Some process of topologies of the beam with a concentrated load are shown in Figs. 1b and 1c, and its optimal topology appears as compression

struts retained between the loading point and the supports, and both ends of the supports are connected by a tie, as shown in Fig. 1d. In the same way, the optimal topology of the beam with a uniform load appears as some compression struts evolved in an arched region, and the supports at both ends are also connected by a tie, as shown in Fig. 2.

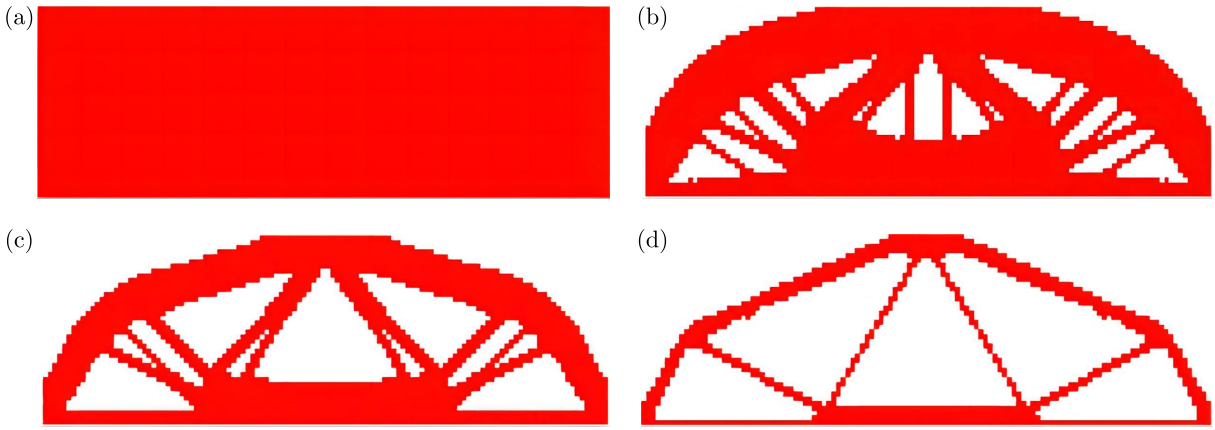

Fig. 1. Topologies of the short beam with an applied concentrated load: (a) initial topology, (b) removal rate of 30%, (c) removal rate of 50%, (d) removal rate of 80%

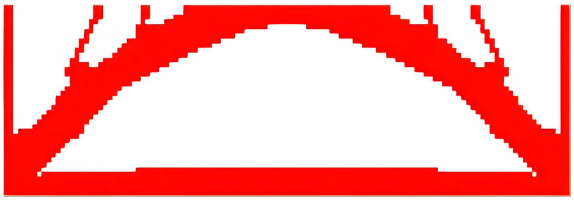

Fig. 2. Optimal topology of the short beam under a uniform load (removal rate 50%)

3. Truss solution to a short beam

3.1. The Michell criterion

The Michell criterion (Michell, 1904; Lewiński *et al.*, 2018) describes an analytical condition of obtaining the optimal structure under certain constraints and loads. Hemp (1973) proved the truss structure which satisfied the Michell criterion would be at a full-stress state, and had the smallest volume and structural compliance. Thus, the stress of member bars in the optimal structure must satisfy the following equation

$$-\sigma_c \leqslant \sigma \leqslant -\sigma_t \tag{3.1}$$

where σ is the stress of member bars in the truss structure, σ_c and σ_t are the permissible stresses of pressure bars and tie-bars, respectively. Meanwhile, the virtual strain $\overline{\varepsilon}$ has the following characteristics

$$\begin{cases} \overline{\varepsilon} = k \operatorname{sgn}\sigma & \text{for} \quad \sigma \neq 0 \\ |\overline{\varepsilon}| \leqslant k & \text{for} \quad \sigma = 0 \end{cases} \tag{3.2}$$

where k is a positive constant, and $\operatorname{sgn}\sigma$ is equal to 1 for tie-bars and -1 for pressure bars.

3.2. Truss solution

In terms of the Michell criterion, the truss appears to be a possible solution to the optimal structure. The truss solution of a structure with different span-depth ratios and a vertically concentrated load in the mid-span are shown in Fig. 3a. It mainly consists of lower arc-shaped tie-bars and pressure bars formed by the straight connection between the loading point and the tie-bars. The arc-shaped tie-bar of the truss solution may be cut off when the design domain is bounded as shown in Fig. 3b. In the meanwhile, Liu and Yi (2013) believed the pressure bars vertically connected with tie-bar would no longer exist when the span-depth ratio was dropping to a certain point. The truss solution to the short beam is shown in Fig. 3c. The pressure bars link the loading point and the supports, and the tie-bars are located on the segmental arc perpendicular to the pressure bars and on the linking line of the supports.

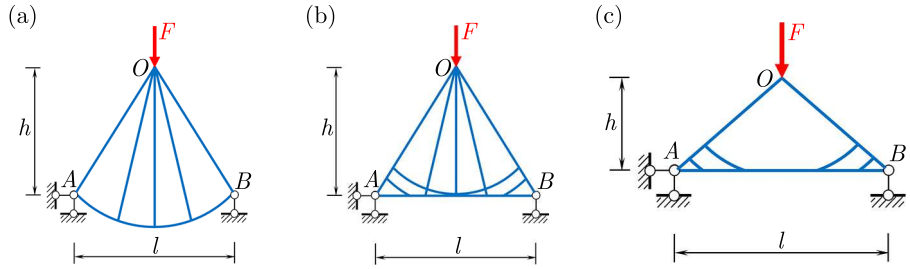

Fig. 3. The truss solutions of structures under a concentrated load: (a) general design domain (Hemp, 1973), (b) bounded design domain (Hemp, 1973), (c) design domain with a small span-depth ratio

The parabolic arch is widely accepted as an optimum structure by the Michell criterion to carry a uniform load between pinned supports. Similarly to the truss solution of a structure under a concentrated load, that under a uniform load needs a tie-bar to transfer tension stress for simple supports, the arc-shaped one will be discontinuous when the design domain is bounded. Besides, the load is transferred through the vertical pressure bars between the loading surface and the arch. The truss solution is shown in Fig. 4.

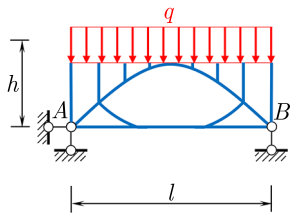

Fig. 4. The truss solutions of a structure under a uniform load

The truss solutions in Fig. 3c and Fig. 4 are highly consistent with the topological solutions shown in Fig. 1d and Fig. 2, respectively. Hence, the ability of TO to obtain a solution with a full-stress state is verified. Furtherly it is reliable to obtain the load-transfer paths by TO to guide structural designs.

4. Nonlinear FEA

4.1. Examples of comparative structure under a concentrated load

4.1.1. Parameters

By completing the nonlinear FEA of the beam and the truss with the ABAQUS, the results were compared for their performance. An overview of the RC short beam without web reinforce-

ment has been introduced in Section 2.2. The reinforcements were aligned in the bottom with a spacing of 40 mm apart, and the cover of reinforcement was 30 mm thick, as shown in Fig. 5a. The 200 mm wide rigid plates were placed at the supports of both ends and loading points to avoid local failure. Correspondingly, a RC triangular truss was designed at the same loading case for contrast, and its boundary was tangent to the beam, as shown is Fig. 5b. The section height of the pressure bars is 250 mm. The layout of the reinforced tie-bars and the rest of parameters are the same as of the beam.

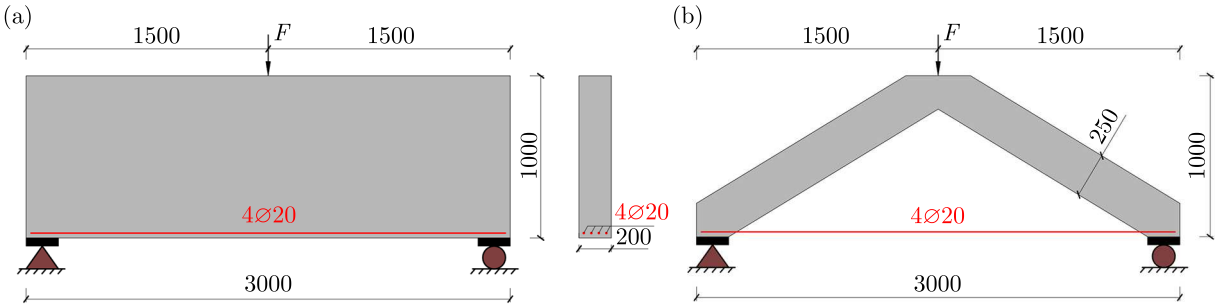

Fig. 5. Dimension and reinforcement layout of two examples (unit: mm): (a) short beam, (b) triangular truss

A concrete damaged plasticity model (Table 1) was applied based on the uniaxial stress-strain curve of concrete recommended by Appendix C of Chinese Code GB 50010-2010 (2016). And the damage factors were introduced to evaluate tensile or compression damage, where 0 indicates no damage and 1 denotes complete damage. The four longitudinal reinforcements were all set 20 mm in diameter and the strength grade was designed with Chinese HRB335: a steel bar with the yield strength of 335 MPa. A double-linear isotropic hardening model was applied in the constitutive model for reinforcement, and the specific parameters are shown in Table 2. Young's elastic modulus and Poisson's ratio of the material are shown in Table 3.

Table 1. Concrete damaged plasticity model

Concrete compression damage				Concrete tension damage			
Compressive behavior		Compression damage		Tensile behavior		Tension damage	
Yield stress	Inelastic strain	Damage parameter	Inelastic strain	Yield stress	Cracking strain	Damage parameter	Cracking strain
20.79	0	0	0	1.421	0	0	0
21.91	0.00058	0.2539	0.00058	1.633	0.000020	0.5156	0.000147
22.80	0.00088	0.4292	0.00144	1.815	0.000025	0.7497	0.000361
21.81	0.00124	0.6286	0.00283	1.947	0.000031	0.8080	0.000495
20.84	0.00144	0.8097	0.00569	2.000	0.000040	0.8784	0.000843
18.59	0.00184	0.8740	0.00839	1.873	0.000066	0.9530	0.002562
16.38	0.00224	0.9117	0.01172	1.683	0.000094		
14.43	0.00263	0.9289	0.01436	1.506	0.000121		
13.57	0.00283	0.9488	0.01963	1.356	0.000147		
10.80	0.00358	0.9564	0.02292	1.231	0.000173		
8.86	0.00430	0.9664	0.02949				
8.10	0.00465	0.9699	0.03277				

The elements used to simulate the concrete and reinforcement were C3D8R and T3D2, which are three-dimensionally reduced integral solid elements with eight nodes, and three-dimensional truss elements with two nodes, respectively. The element sizes of the concrete and reinforcement

Table 2. Plasticity parameters of the reinforcement

Yield stress	Plastic strain
335	0
335	0.1

Table 3. Material properties

Parameter	Young's modulus [N/mm^2]	Poisson's ratio [–]
Concrete	29791.5	0.2
Reinforcement	200000	0.3
Rigid plate	200000	0.3

were 50 mm and 30 mm, respectively. The elements were intensified at the nodes of the truss. Besides, in element meshing of the modeling, the concrete at the node area was cut out firstly and then meshed into a hexahedral element with an approximate size of 25 mm.

The concrete and the steel bars were set as embedding constraints. The loading point was coupled with concrete on the top surface of the beam. Rotational freedom of the loading point in two directions was fixed to avoid out-of-plane rotation. In addition, the displacement loading was adopted to ensure convergence.

4.1.2. Results

(1) Concrete stress and damage of the short beam

The von Mises stress nephogram of concrete in the beam is shown in Fig. 6a, and the tensile damage herein is shown in Fig. 6b. We draw the truss upon the tensile damage diagram, and the beam can be divided into four parts: area I, area II, truss area and damage area, as shown in Fig. 6c. According to Fig. 6a, obviously, the stress in area I and area II of Fig. 6c is at a

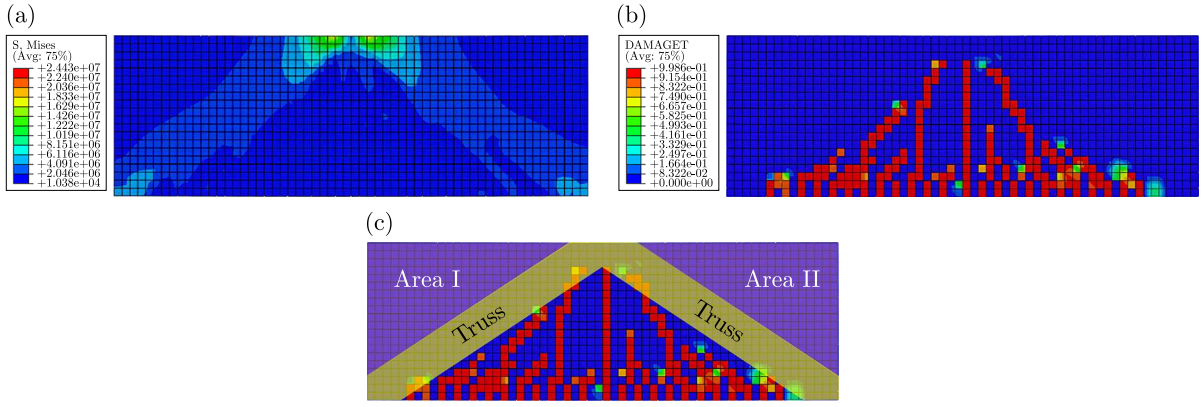

Fig. 6. Stress and tensile damage of the concrete of short beam under a concentrated load: (a) von Mises stress distribution of concrete, (b) tensile damage of concrete, (c) area division by distribution of stress and tensile damage

relatively low level, even close to 0 MPa, i.e., the materials herein are not fully utilized. This phenomenon can explain itself with Saint Venant's principle as well. According to Fig. 6b, the concrete cracks, including vertical bending cracks in the mid-span and diagonal cracks between the supports and the loading point, form a triangular tensile damage area in Fig. 6c. For cracking in this area, the concrete withdrawal from the tensile work and its stress are also relatively low, and this can also be seen from Fig. 6a. The truss area in Fig. 6c is completely located in the

high-stress area of Fig. 6a, in which most of the elements have von Mises stress between 8 MPa and 14 MPa. A few cracks also exist in this area as shown in Fig. 6b. Therefore, it is proved again that the truss is the core frame of the beam under a concentrated load.

(2) Reinforcement stress

The tensile stress distribution of reinforcements is shown in Fig. 7. The von Mises stress of longitudinal reinforcements in the beam ranges from 150 MPa to 170 MPa, while in the tie-bars of the truss, from 182 MPa to 189 MPa. Thus, the average reinforcement stress level of the beam is only 10%-15% lower than that of the truss. In addition, except for the nodes, the stress in the whole length of truss tie-bars is much more evenly distributed because of the absence of concrete, and the ratio of tension length to total length of the reinforcement is higher than that of the beam.

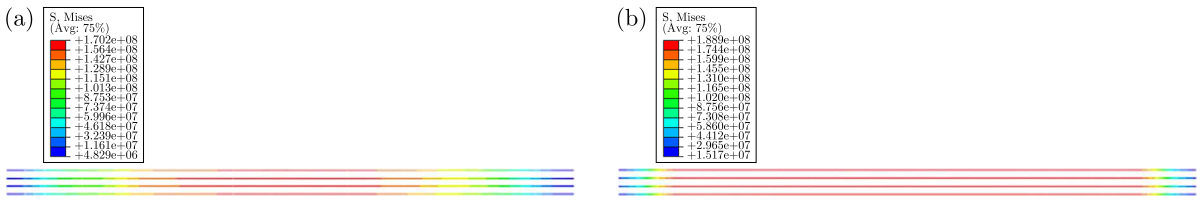

Fig. 7. Stress of reinforcements of two examples under a concentrated load: (a) short beam, (b) triangular truss

(3) Mid-span deflection

The load-deflection curves of the two examples are shown in Fig. 8. The mid-span deflection of the truss is 2.38 mm when the load is 340 kN, and it increases linearly with the load, which indicates that the truss is at the elastic stage. On the other hand, the mid-span deflection of the beam increases nonlinearly with the accumulation of concrete damage, and finally reaches 1.59 mm, which is 2/3 of the truss and far less than the limit value of 14 mm specified in the current Chinese Code GB 50010-2010 (2016). It can be concluded that the concrete part of the beam, the truss area excluded, has considerable significance to the stiffness of the structure.

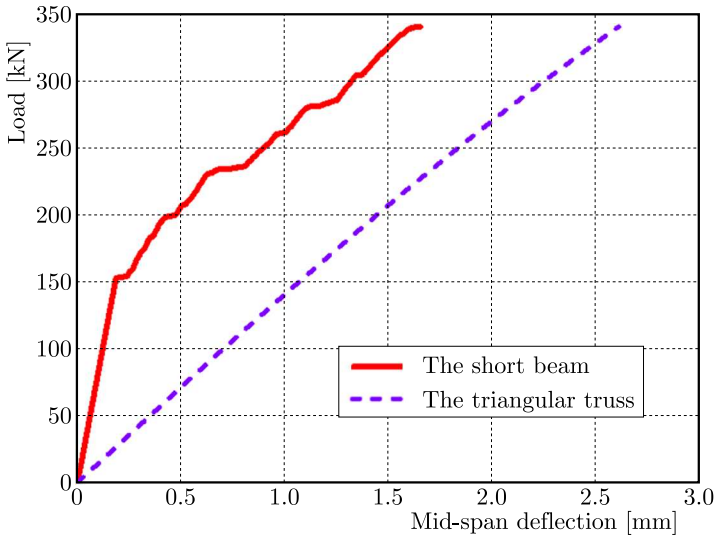

Fig. 8. Load-deflection curves of two examples under a concentrated load

4.2. Examples of the comparative structure under a uniform load

4.2.1. Parameters

The load of the short beam was changed to a uniform load on the top. Besides, a RC tie--arch was designed at the same loading case for contrast, and its boundary was also tangent to the beam as shown in Fig. 9. The section height of the main arch ring was 200 mm. For the concrete arch, element meshing was carried out along the external edge with an approximate size of 50 mm. The design of the reinforced tie-bars and the rest of parameters were the same as of the truss in Section 4.1.1.

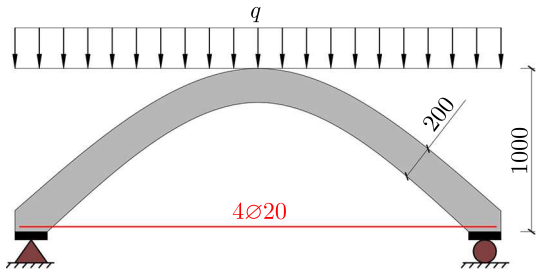

Fig. 9. Dimension and reinforcement layout of tie-arch examples (unit: mm)

4.2.2. Results

(1) Concrete stress and damage of the short beam

The von Mises stress nephogram of concrete in the beam is shown in Fig. 10a, and tensile damage in Fig. 10b. In the same way as in Section 4.1.2, the arch is drawn upon the tensile damage diagram and the beam is divided into four parts as shown in Fig. 10c. In a similar way, the arch area in Fig. 10c is completely located in the high-stress area of Fig. 10a, in which most of the elements have von Mises stress between 5 MPa and 11 MPa. Thus, the arch is actually the core frame of the beam under a uniform load.

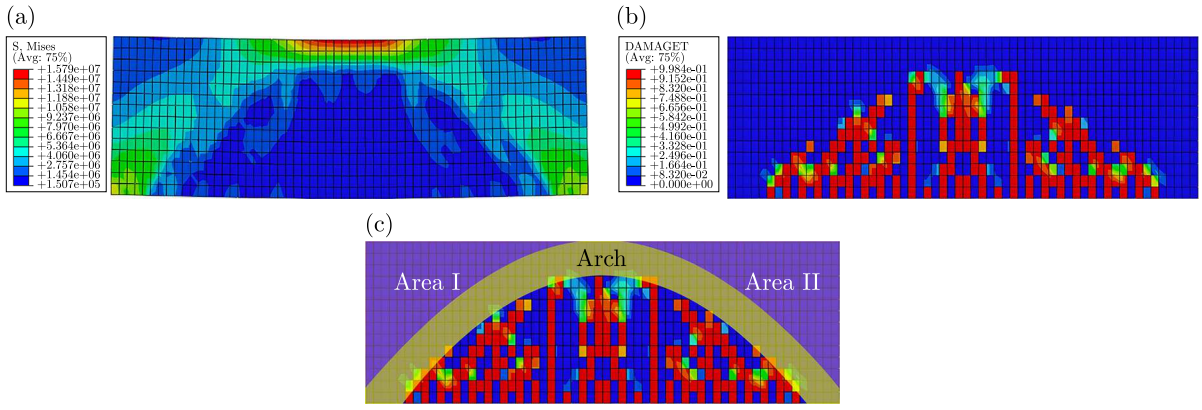

Fig. 10. Stress and tensile damage of concrete of the short beam under a uniform load: (a) von Mises stress distribution of concrete, (b) tensile damage of concrete, (c) area division by distribution of stress and tensile damage

(2) Reinforcement stress

The tensile stress distribution of the reinforcements is shown in Fig. 11. The maximum von Mises stress of longitudinal reinforcement occurring in the middle of the beam is 230 MPa, as shown in Fig. 11a, while that in the arch tie-bars is close to the yield strength of 290 MPa, as shown in Fig. 11b. The stress of the arch tie-bars in the whole length (the part near the nodes

excluded) is relatively evenly distributed, and its average level is only 20% higher than that of the beam.

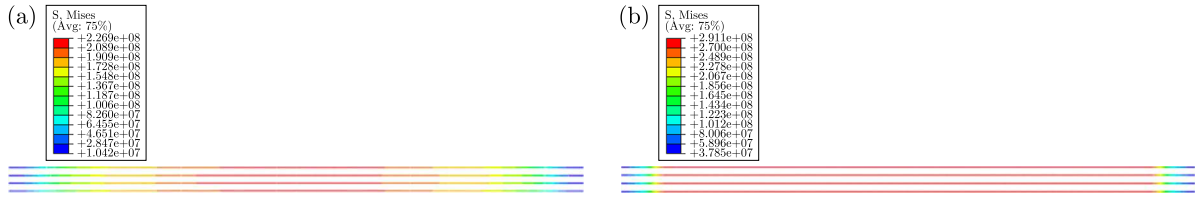

Fig. 11. Stress of reinforcement of two examples under a uniform load: (a) short beam, (b) tie arch

(3) Mid-span deflection

The load-deflection curves of the two examples are shown in Fig. 12. The tie-arch basically is kept at the elastic stage and its deflection finally reaches 3.59 mm at 1500 kN/m^2, while the increasing law of deflection of the beam herein is almost the same as it is under a concentrated load in Section 4.1.3. The ultimate deflection of the beam is about 63% of that of the tie-arch, and hence the concrete part of the beam (arch area excluded) has made a significant contribution to stiffness of the structure.

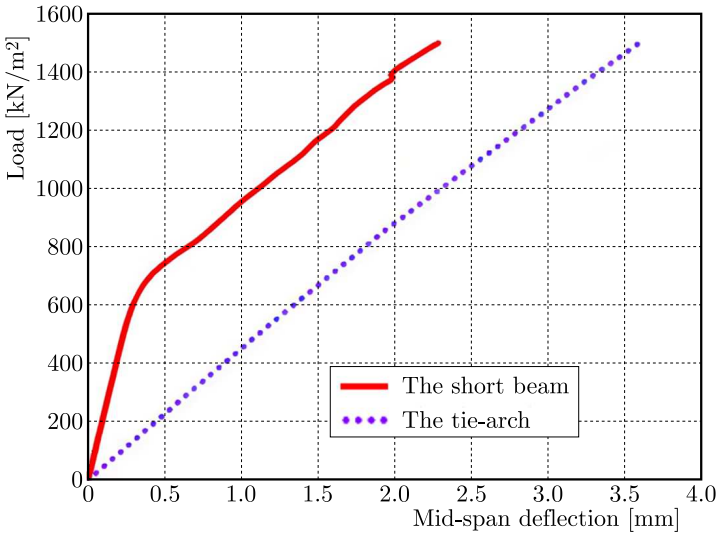

Fig. 12. Load-deflection curve of two examples under a uniform load

In general, the core frames of the short beam at both ends are a triangle truss and tie-arch when applying a concentrated load and a uniform load, respectively, which can be regarded as the load-transfer path as well. Therefore, the RC short beam can be respectively designed as a truss or a tie-arch according to practical projects when a concentrated load or a uniform load is applied to it, so as to strengthen a part of load-transfer paths and weaken the rest parts with lower stresses.

5. Discussions on load-transfer paths

5.1. Topology solution and load-transfer paths

The elements of topology solutions of the simply supported short beam under a concentrated load and a uniform load are mainly distributed on the path lines of principal tensile stress and main compression stress (as shown in Fig. 1d and Fig. 2), which indicates the load-transfer paths of the RC members.

In addition, these two topologies coincide with the high-stress area of the short beams presented in Section 4. The process of evolution of the short beam into the triangle truss under a concentrated load and into the tie-arch under a uniform load are revealed in Fig. 1 and Fig. 2, respectively. It verifies that the two structures are the core frame of the short beam at different loading cases, and this frame as the load-transfer paths of the members can be obtained by topology optimization (TO).

5.2. Design suggestion for the short beam

After the load-transfer paths are constructed through TO, three main ways are available to implement design guidance.

The first way is about the aided design based on STM. Small conventional concrete structural members always have simple shapes, and hence it is feasible to transform their load-transfer paths into STMs and then to carry on the design based on STM analysis. The materials outside the load-transfer paths can be ignored in mechanical analysis since STMs are essentially truss models. Still, these parts of the materials contribute to structural stiffness, and naturally they cannot be removed in the construction. Specifically, when a concentrated load is applied to the short beam, the design procedure of such a type of members is summarized as follows:

- Transform the load-transfer paths into STMs which are composed of ties, struts and nodes according to calculations or FEA results (in Fig. 13).
- Calculate the bearing capacity of the nodes according to different node types of CCC, CCT and CTT, in which C denotes compression and T denotes tension.
- Calculate the height of the compression area based on the balance of the moment and horizontal force.
- Design the amount and layout of the reinforcements based on mechanical calculation results of the ties.
- Check the strength of the struts and the nodes.
- Add constructional reinforcements, such as distribution reinforcements, anchorage extension for tie reinforcements, and so on.

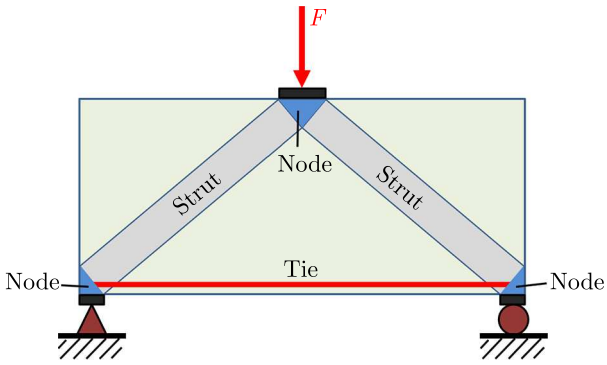

Fig. 13. STM of the short beam with a concentrate load applied

The second is about the direct reference to the design. In large concrete structural members, like box girders, the materials outside the part in load-transfer paths can be removed after TO, then a part in the load-transfer paths can be quantified according to the load, bearing capacity target or stiffness target. This design can allow a more efficient use of materials and greatly reduce the self-weight of the structures.

The third way is about the design based on 3D printing technology. It is bound to make on-site construction infeasible for some special concrete structural members since a part or all of materials outside the part of load-transfer paths needs to be removed according to the topological

solution due to functional requirements or some other reasons. 3D printing technology can be used to make a special concrete formwork, or factory components prefabrication for the on-site assembly. Anyway, further comprehensive researches are needed to find the optimal design of short beams.

6. Conclusions

- The load-transfer paths in short beams without web reinforcement under a specified load can be directly evolved through TO. The result and force mechanism of the short beams are supported by the Michell criterion.
- The triangle truss and the tie-arch are the core frame. They reveal the main load-transfer paths of the short beams under a concentrated and uniform load, respectively.
- In the short beams, the distribution of high-stress compression area appears as a truss under a concentrated load and a tie-arch under a uniform load. The truss and tie-arch have almost the same bearing capacity and, meanwhile, can save many more materials since the materials are fully utilized.
- For some small conventional concrete structural members with simple shapes, the load--transfer paths obtained by TO can be transformed into STMs. The amount and layout of the reinforcements are designed based on mechanical calculation results of the ties.
- For large concrete structural members, the reinforcement in load-transfer paths can be calculated quantitatively, and the materials outside the paths can be removed. For special concrete structural members, 3D printing technology can be used to make the formwork and to arrange reinforcement or the steel pipe in the tensile area.

In addition, more experiments are needed to compare with the examples and verify the load--transfer paths for the design method of RC short beams in future research, and then promote the development of universal design concepts.

Acknowledgements

The work described in this paper was fully funded by the National Science Foundation of China (grant No. 51508182) and the Natural Science Foundation of Hunan Province, China (grant No. 2021JJ30270).

References

1. ACI (American Concrete Institute) Committee 318, 2019, Building code requirements for structural concrete and commentary, (ACI 318-19), Farmington Hills, MI: ACI
2. Bendsøe M.P., 1989, Optimal shape design as a material distribution problem, *Structural and Multidisciplinary Optimization*, **1**, 4, 193-202
3. Bendsøe M.P., Kikuchi N., 1988, Generating optimal topologies in structural design using a homogenization method, *Computer Methods in Applied Mechanics and Engineering*, **71**, 2, 197-224
4. Bendsøe M.P., Sigmund O., 2003, Extensions and applications, [In:] *Topology Optimization*, Springer, Berlin, 71-158
5. Chen H., Yi W.J., Hwang H.J., 2018, Cracking strut-and-tie model for shear strength evaluation of reinforced concrete deep beams, *Engineering Structures*, **163**, May 15, 396-408
6. Chinese Code GB 50010-2010, 2016, *Code for Design of Concrete Structures*, Ministry of Housing and Urban-Rural Development of the People's Republic of China 2016, Beijing, China (in Chinese)
7. Díaz R.A.S., Sarmiento Nova S.J.S., Teixeira da Silva M.C.A., Trautwein L.M., de Almeida L.C., 2020, Reliability analysis of shear strength of reinforced concrete deep beams using NLFEA, *Engineering Structures*, **203**, 109760

8. Dorn W.S., Gomory R.E., Greenberg H.J., 1964, Automatic design of optimal structures, *Journal de Mécanique*, **3**, 25-52
9. Hemp W.S., 1973, *Optimum Structure*, Clarendon Press, Oxford
10. Huang X., Xie Y.M., 2007, Numerical stability and parameters study of an improved bi-directional evolutionary structural optimization method, *Structural Engineering and Mechanics*, **27**, 1, 49-61
11. Ismail K.S., Guadagnini M., Pilakoutas K., 2018, Strut-and-tie modeling of reinforced concrete deep beams, *Journal of Structural Engineering*, **144**, 2, 04017216
12. Jewett J.L., Carstensen J.V., 2019, Experimental investigation of strut-and-tie layouts in deep RC beams designed with hybrid bi-linear topology optimization, *Engineering Structures*, **197**, 109322
13. Kotsovos M.D., 1988, Compressive force path concept: basis for reinforced concrete ultimate limit state design, *Structural Journal*, **85**, 1, 68-75
14. Lewiński T., Sokół T., Graczykowski C., 2018, *Michell Structures*, Springer, Berlin
15. Liu X., Yi W.J., 2013, Construction of strut-and-tie model for reinforced concrete beams by optimal method, *Engineering Mechanics*, **30**, 9, 151-157
16. Magnucki K., Malinowski M., Magnucka-Blandzi E., Lewiński J., 2017, Three-point bending of a short beam with symmetrically varying mechanical properties, *Composite Structures*, **179**, 552-557
17. Michell A.G.M., 1904, The limits of economy of material in frame structure, *The London, Edinburgh, and Dublin Philosophical Magazine and Journal of Science*, **8**, 47, 589-597
18. Querin O.M., Steven G.P., Xie Y.M., 1998, Evolutionary structural optimization (ESO) using a bidirectional algorithm, *Engineering Computations*, **15**, 8, 1031-1048
19. Querin O.M., Young V., Steven G.P., Xie Y.M., 2000, Computational efficiency and validation of bi-directional evolutionary structural optimization, *Computer Methods in Applied Mechanics and Engineering*, **189**, 2, 559-573
20. Rombach G.A., 2011, *Finite Element Design of Concrete Structures*, Ice Publishing, London
21. Uenaka K., Tsunokake H., 2017, Behavior of concrete filled elliptical steel tubular deep beam under bending-shear, *Structures*, **10**, 89-95
22. Xia L., Xia Q., Huang X., Xie Y.M., 2018, Bi-directional evolutionary structural optimization on advanced structures and materials: a comprehensive review, *Archives of Computational Methods in Engineering*, **25**, 2, 437-478
23. Xie Y.M., Steven G.P., 1993, A simple evolutionary procedure for structural optimization, *Computers and Structures*, **49**, 5, 885-896
24. Yang X.Y., Xie Y.M., Liu J.S., Parks G.T., Clarkson P.J., 2002, Perimeter control in the bidirectional evolutionary optimization method, *Structural and Multidisciplinary Optimization*, **24**, 6, 430-440

Manuscript received April 27, 2022; accepted for print September 14, 2022